

AD _____
(Leave blank)

Award Number: W81XWH-09-1-0025

TITLE: Early Assessment of Breast Cancer Therapy Response
Using Photoacoustic Molecular Imaging

PRINCIPAL INVESTIGATOR: Adam de la Zerda, BSc, MSc

CONTRACTING ORGANIZATION: LELAND STANFORD JUNIOR UNIVERSITY
STANFORD, CA 94305-5014

REPORT DATE: January 2011

TYPE OF REPORT: Annual Summary

PREPARED FOR: U.S. Army Medical Research and Materiel Command
Fort Detrick, Maryland 21702-5012

DISTRIBUTION STATEMENT: (Check one)

- ☒ Approved for public release; distribution unlimited
- ☐ Distribution limited to U.S. Government agencies only;
report contains proprietary information

The views, opinions and/or findings contained in this report are those of the author(s) and should not be construed as an official Department of the Army position, policy or decision unless so designated by other documentation.

REPORT DOCUMENTATION PAGE			<i>Form Approved</i> OMB No. 0704-0188	
<small>Public reporting burden for this collection of information is estimated to average 1 hour per response, including the time for reviewing instructions, searching existing data sources, gathering and maintaining the data needed, and completing and reviewing this collection of information. Send comments regarding this burden estimate or any other aspect of this collection of information, including suggestions for reducing this burden to Department of Defense, Washington Headquarters Services, Directorate for Information Operations and Reports (0704-0188), 1215 Jefferson Davis Highway, Suite 1204, Arlington, VA 22202-4302. Respondents should be aware that notwithstanding any other provision of law, no person shall be subject to any penalty for failing to comply with a collection of information if it does not display a currently valid OMB control number. PLEASE DO NOT RETURN YOUR FORM TO THE ABOVE ADDRESS.</small>				
1. REPORT DATE 31-01-2011		2. REPORT TYPE Annual Summary		3. DATES COVERED (From - To) 1 Jan 2010 - 31 Dec 2010
4. TITLE AND SUBTITLE Early Assessment of Breast Cancer Therapy Response Using Photoacoustic Molecular Imaging		5a. CONTRACT NUMBER W81XWH-09-1-0025		
		5b. GRANT NUMBER		
		5c. PROGRAM ELEMENT NUMBER		
6. AUTHOR(S) Adam de la Zerda adlz@stanford.edu		5d. PROJECT NUMBER		
		5e. TASK NUMBER		
		5f. WORK UNIT NUMBER		
7. PERFORMING ORGANIZATION NAME(S) AND ADDRESS(ES) LELAND STANFORD JUNIOR UNIVERSITY STANFORD, CA 94305-5014		8. PERFORMING ORGANIZATION REPORT NUMBER U.S. Army Medical Research and Materiel Command Fort Detrick, Maryland 21702-5012		
9. SPONSORING / MONITORING AGENCY NAME(S) AND ADDRESS(ES) U.S. Army Medical Reserach and Materiel Command Ft. Detrick, MD 21702		10. SPONSOR/MONITOR'S ACRONYM(S)		
		11. SPONSOR/MONITOR'S REPORT NUMBER(S)		
12. DISTRIBUTION / AVAILABILITY STATEMENT Approved for public release; distribution unlimited				
13. SUPPLEMENTARY NOTES				
14. ABSTRACT The purpose of this grant is to build instrumentation and imaging agents for photoacoustic imaging of breast cancer, using which one could estimate the change in molecular expression of various breast-cancer-specific proteins undergoing chemotherapy treatment. We've made significant progress towards obtaining this goal: 1) we have adapted our instrumentation hardware and image reconstruction software for allowing to acquire photoacoustic images of multiple contrast agents simultaneously; 2) We developed several new contrast agents based on carbon nanotubes and showed they exhibit 300-times higher sensitivity and for the first allow imaging photoacoustic molecular probes at sub-nanomolar concentrations (one paper published in Nano Letters and another was submitted to Nano Letters as well).				
15. SUBJECT TERMS Photoacoustic Imaging, Molecular Imaging				
16. SECURITY CLASSIFICATION OF:			17. LIMITATION OF ABSTRACT UU	18. NUMBER OF PAGES 32
a. REPORT U	b. ABSTRACT U	c. THIS PAGE U		
				19b. TELEPHONE NUMBER (include area code)

Table of Contents

	<u>Page</u>
Introduction.....	4
Body.....	4
Key Research Accomplishments.....	9
Reportable Outcomes.....	9
Conclusion.....	9
References.....	9
Appendices.....	10

1. INTRODUCTION

The purpose of this grant is to build instrumentation and imaging agents for photoacoustic imaging of breast cancer, using which one could estimate the change in molecular expression of various breast-cancer-specific proteins undergoing chemotherapy treatment. We've made significant progress towards obtaining this goal: 1) we have adapted our instrumentation hardware and image reconstruction software for allowing to acquire photoacoustic images of multiple contrast agents simultaneously; 2) We developed 5 new contrast agents based on carbon nanotubes and showed they exhibit 300-times higher sensitivity and for the first allow imaging photoacoustic molecular probes at sub-nanomolar concentrations (one paper published in Nano Letters and another was submitted to Nano Letters as well).

2. BODY

2.1 Major training milestones

Over the course of the last 2 years I have achieved most of the training milestones I have set for myself at the beginning of the training grant as well as others. As the previous yearly report did not include the training milestones, this report will cover both 2009 and 2010. These training milestones include: yearly participation and giving oral presentations in the World Molecular Imaging Congress (in 2009 and 2010), participation in the Photonics West 2009 conference (and being awarded the Best Poster Award in the Photoacoustic Imaging category), participating and presenting my work at the Canary Cancer Early Detection Symposium of 2009 and 2010. For the last 2 years, I have mentored three undergraduate and high-school students (Sunil Bodapati, Robert Teed and Salomon May) in summer research activities, all of these summer internships resulted in research papers related to Photoacoustic cancer imaging. Furthermore, I have spent over 30 days shadowing physicians in the clinic and surgical rooms, including Dr. Irene Wapnir (Breast Cancer Surgery), Dr. Dean Felsner (Oncology) and others. I have regularly attended the bi-weekly journal clubs, weekly Nuclear Medicine clinical grand rounds, weekly Gambhir group lab meetings, Monthly Molecular Imaging Seminar Series and Monthly Nanobiotechnology Seminar Series, all of which greatly influenced my basic science and clinical understanding of cancer and reaffirmed my desire to pursue a career as an

independent investigator focusing on developing molecular imaging techniques for cancer patients, particularly breast cancer.

2.2 Developing new instrumentation hardware and image reconstruction software for allowing multiplexing studies of more than one photoacoustic imaging agents.

Last year we reported on two new photoacoustic imaging agents we developed based on single walled carbon nanotubes (SWNTs) conjugated to optical dyes (Indocyanine green and QSY₂₁). However, in order to allow each of these imaging agents to report on a different molecular activity in a tumor, instrumentation that allows multiplexing has to be in place. We have adapted our photoacoustic imaging instrument to allow multiple-wavelength acquisition between the wavelengths of 690 to 900 nm. We have then adapted the image reconstruction algorithm to calculate the photoacoustic spectrum of each voxel in the three-dimensional (3D) photoacoustic image and using least squares, calculate the relative amount of each of the imaging agents in this voxel. The algorithm then produces new 3D photoacoustic images representing the distribution of the imaging agent in the image (i.e., spectral unmixing the image to its spectral components). We tested this algorithm both in phantoms (**Fig. 1**) as well as in living animals (**Fig. 2**) and received very encouraging results, which we have submitted as a research paper to Nano Letters (see submitted manuscript in the appendix). Importantly, this is the very first time where true multiplexing capabilities are demonstrated with photoacoustic imaging.

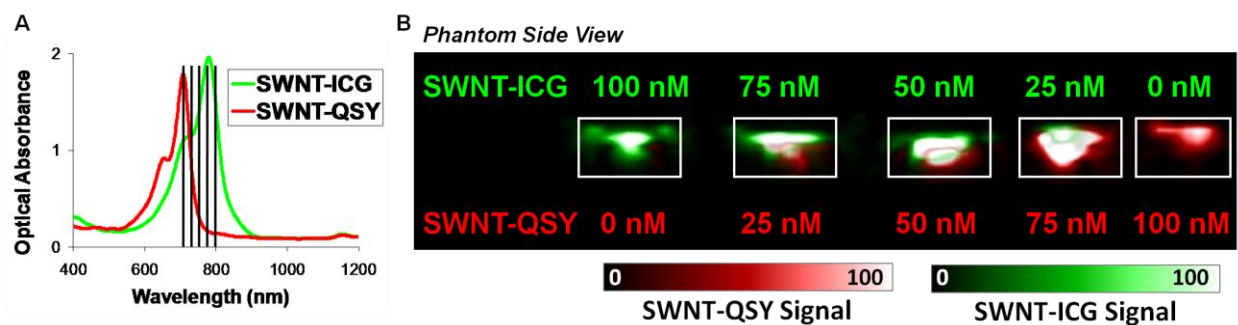


Figure 1. Multiplexing of SWNT-QSY with SWNT-ICG *in-vitro*. (A) An agarose phantom containing SWNT-ICG and SWNT-QSY at different mixture concentrations (pure SWNT-ICG, 1:3, 1:1, 3:1 and pure SWNT-QSY) was scanned using the photoacoustic instrument at 5 different wavelengths (at 700, 730, 760, 780, 800 nm). (B) Despite their overlapping spectra, the photoacoustic signals from SWNT-QSY and SWNT-ICG were unmixed.

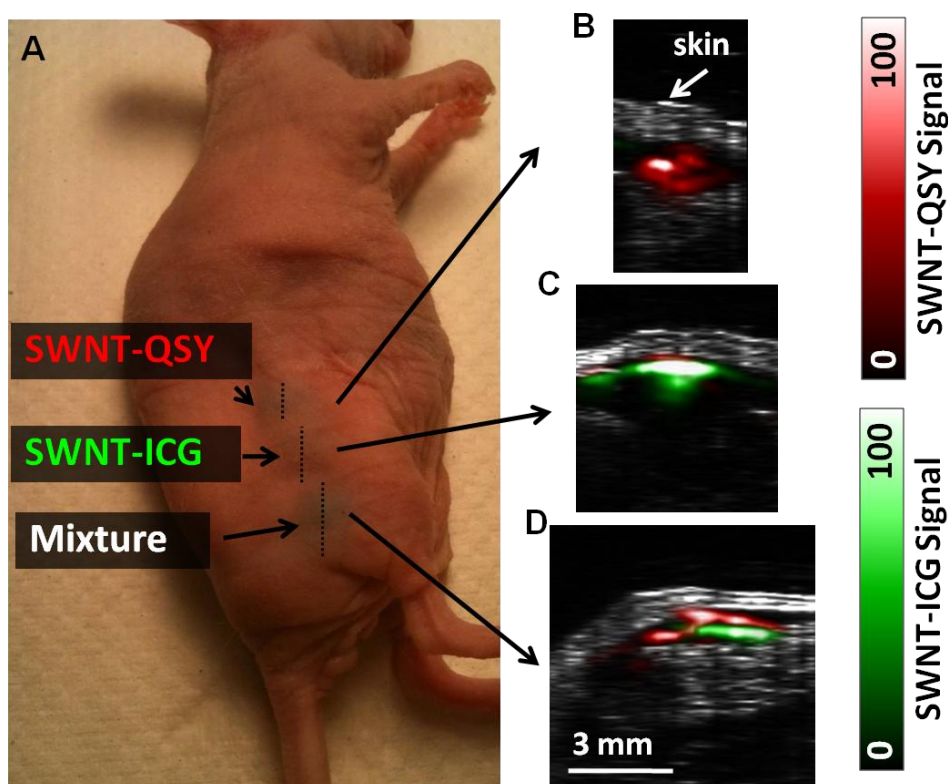
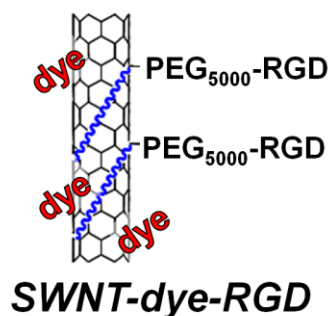


Figure 2. Multiplexing of SWNT-QSY with SWNT-ICG in living mice. (A) Mouse injected with 30 μ l of 50 nM SWNT-QSY (upper inclusion), 30 μ l of 50 nM SWNT-ICG (middle inclusion) and 30 μ l of an equal mixture of 50 nM of SWNT-QSY and SWNT-ICG (lower inclusion). (B) The unmixed photoacoustic vertical slice through the upper inclusion, showing only red signal from the SWNT-QSY. (C) The unmixed photoacoustic slice through the middle inclusion, showing mostly green signal from the SWNT-ICG. (D) The unmixed photoacoustic slice through the lower inclusion, showing both red and green signals of SWNT-QSY and SWNT-ICG spread throughout the inclusion area. Image reconstruction artifacts as well as inhomogeneous light penetration into the tissue are likely the cause for the separation of the green and red signals in the image. (E) The wavelengths used for the photoacoustic scans were 700, 730, 760, 780, 800 nm.

2.3 Development of 3 additional photoacoustic molecular imaging agents.

In addition to the SWNT-ICG and SWNT-QSY imaging agents, we have further exploited the π - π interactions of optical dyes with the hydrophobic surface of the single walled carbon nanotubes (SWNTs), and synthesized 3 additional photoacoustic molecular imaging agents. The dyes we attached were Cy5.5, Methylene Blue, and Melanin, all of which produced a distinct optical absorbance spectra for a photoacoustic instrument to detect (Fig 3, see submitted manuscript in the appendix).

A



B

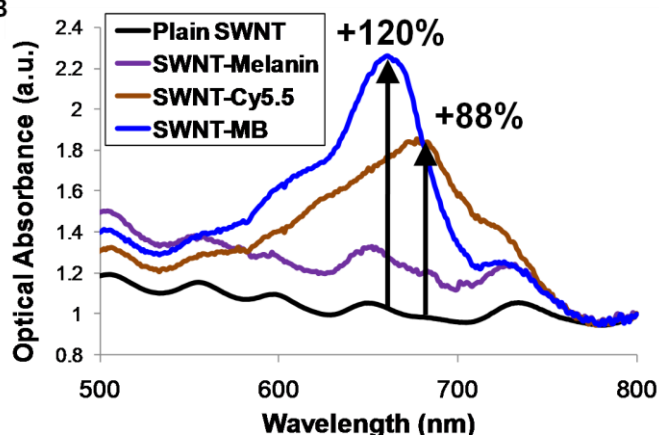


Figure 3. Characterization of the dye-enhanced SWNT. (A) Illustration of a SWNT-dye construct that is targeted to tumor angiogenesis through RGD peptides conjugated to polyethylene glycol (PEG) chains. **(B)** Optical absorbance spectra of the SWNT-dye conjugates for the dyes of Melanin (purple), Cy5.5 (brown) and Methylene Blue (blue).

2.4 Demonstrating of tumor targeting of SWNT-ICG and SWNT-QST photoacoustic imaging agents.

For the two newly developed photoacoustic imaging agents (SWNT-ICG and SWNT-QSY), we have attached an RGD peptide to their surface and demonstrated that despite their higher weight, they still preserved the excellent tumor targeting capabilities as plain SWNTs, while demonstrating great in-vivo sensitivity of over 300-times better than plain SWNTs (**Fig. 4**, see paper in appendix that was published in 2010 in Nano Letters).

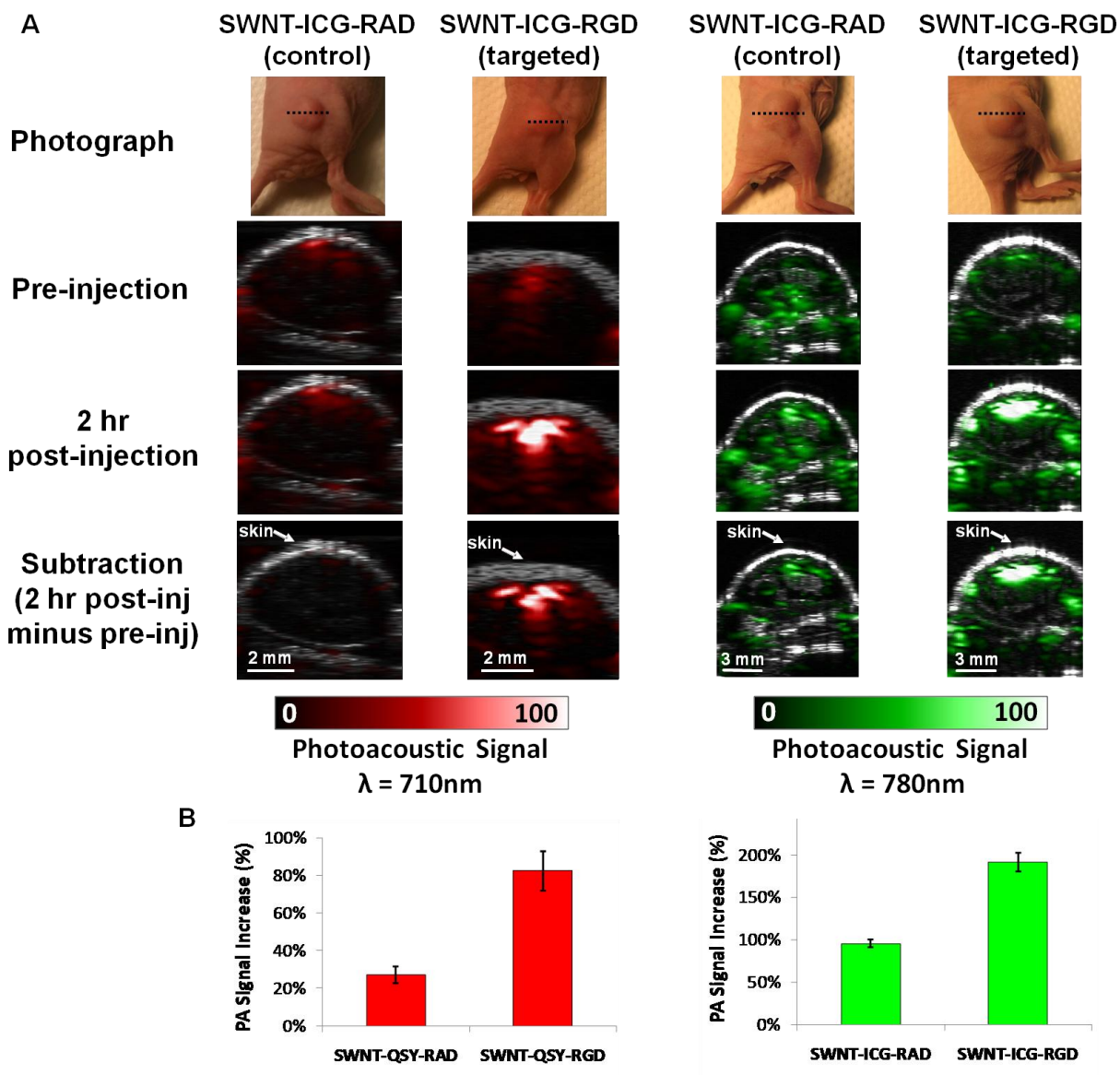


Figure 4. Dye-SWNT tumor targeting in living mice. (A) Ultrasound (gray) and photoacoustic (red for $\lambda = 710\text{ nm}$ and green for $\lambda = 780\text{ nm}$) images of a vertical slice through the tumors (dotted black line). The ultrasound images show the skin and the tumor boundaries. Subtraction photoacoustic images were calculated as 2 hr post-injection minus pre-injection images. As can be seen in the subtraction images, SWNT-QSY-RGD as well as SWNT-ICG-RGD accumulate in significantly higher amounts in the tumor as compared to their respective control particles. **(B)** Quantitative region-of-interest analysis shows that SWNT-QSY-RGD creates a 3-fold higher photoacoustic signal increase in the tumor than the control SWNT-QSY-RAD particle ($p < 0.01$). SWNT-ICG-RGD provides over 100% higher photoacoustic signal increase than the control SWNT-ICG-RAD ($p < 0.01$). The error bars represent standard error ($n = 3$ mice).

3. KEY RESEARCH ACCOMPLISHMENTS

- Developed instrumentation hardware and image reconstruction software to allow imaging of multiple photoacoustic imaging agents simultaneously in living mice.
- Finished the development of a total of 6 photoacoustic imaging agents.
- Demonstrated the photoacoustic imaging agents can target tumors in living mice upon intravenous injection at sub-nanomolar sensitivities.

4. REPORTABLE OUTCOMES

- **Paper submitted: Adam de la Zerda**, Sunil Bodapati, Robert Teed, Salomon May, Scott Tabakman, Zhuang Liu, Butrus Khuri-Yakub, Xiaoyuan Chen, Hongjie Dai, Sanjiv S. Gambhir, “Family of Enhanced Photoacoustic Imaging Agents for High Sensitivity and Multiplexing Studies in Living Mice”, *submitted to Nano Letters*.
- **Paper published: Adam de la Zerda***, Zhuang Liu*, Sunil Bodapati, Robert Teed, Srikant Vaithilingam, Butrus Khuri-Yakub, Xiaoyuan Chen, Hongjie Dai, Sanjiv S. Gambhir, “Ultrahigh Sensitivity Carbon Nanotube Agents for Photoacoustic Molecular Imaging in Living Mice”, *In Press for Nano Letters* (2010) (*equal contribution).
- **Abstract submitted: Adam de la Zerda**, Sunil Bodapati, Shay Keren, Cristina Zavaleta, Robert Teed, Zhuang Liu, Scott Tabakman, Srikant Vaithilingam, Xiaoyuan Chen, Butrus T. Khuri-Yakub, Hongjie Dai, Sanjiv Sam Gambhir, “Photoacoustic Molecular Imaging using Carbon Nanotubes for Ultra-high Sensitivity Imaging of Breast Cancer In-vivo”, submitted to *Era of Hope* (2011)
- **Abstract presented: Adam de la Zerda**, Sunil Bodapati, Robert M. Teed, Scott Tabakman, Zhuang Liu, Butrus T. Khuri-Yakub, Xiaoyuan Chen, Hongjie Dai, Sanjiv Sam Gambhir “Family of enhanced photoacoustic imaging agents for high sensitivity and multiplexing studies in living mice”, World Molecular Imaging Congress (2010).

5. CONCLUSION

The main achievement over this past year was the development of 3 additional new photoacoustic imaging agents which allow reaching unprecedented sensitivities, adaptation of the photoacoustic instrument to allow true multiplexing studies in vitro as well as in animals, and finally, the demonstration of the tumor targeting of the new SWNT-based imaging agents.

6. REFERENCES

N/A

1. Paper published in Nano Letters:

Ultrahigh Sensitivity Carbon Nanotube Agents for Photoacoustic Molecular Imaging in Living Mice

Adam de la Zerda,^{†,‡,¶} Zhuang Liu,^{§,‡,¶} Sunil Bodapati,[†] Robert Teed,[†] Srikant Vaithilingam,[‡] Butrus T. Khuri-Yakub,[‡] Xiaoyuan Chen,^{†,¶} Hongjie Dai,^{*,§} and Sanjiv Sam Gambhir^{*,†,||}

[†]Molecular Imaging Program at Stanford, Department of Radiology and Bio-X Program, [‡]Department of Electrical Engineering, [§]Department of Chemistry, and ^{||}Department of Bioengineering, Stanford University, Palo Alto, California 94305, [‡]Functional Nano & Soft Materials Laboratory (FUNSOM), Soochow University, Suzhou, Jiangsu, 215123, China, and [¶]Laboratory for Molecular Imaging and Nanomedicine, National Institute of Biomedical Imaging and Bioengineering (NIBIB), National Institutes of Health (NIH), Bethesda, Maryland 20892, USA

ABSTRACT Photoacoustic imaging is an emerging modality that overcomes to a great extent the resolution and depth limitations of optical imaging while maintaining relatively high-contrast. However, since many diseases will not manifest an endogenous photoacoustic contrast, it is essential to develop exogenous photoacoustic contrast agents that can target diseased tissue(s). Here we present a novel photoacoustic contrast agent, Indocyanine Green dye-enhanced single walled carbon nanotube (SWNT-ICG). We conjugated this contrast agent with cyclic Arg-Gly-Asp (RGD) peptides to molecularly target the $\alpha_v\beta_3$ integrins, which are associated with tumor angiogenesis. Intravenous administration of this tumor-targeted contrast agent to tumor-bearing mice showed significantly higher photoacoustic signal in the tumor than in mice injected with the untargeted contrast agent. The new contrast agent gave a markedly 300 times higher photoacoustic contrast in living tissues than previously reported SWNTs, leading to subnanomolar sensitivities. Finally, we show that the new contrast agent can detect ~ 20 times fewer cancer cells than previously reported SWNTs.

KEYWORDS Photoacoustic molecular imaging, carbon nanotube

Photoacoustic imaging is an emerging modality based on the photoacoustic effect where light is converted into ultrasound waves that are detected outside the subject of interest.¹ Photoacoustic imaging has been used in numerous applications where intrinsic contrast is available such as visualizing blood vessels structure,² thermal burns,³ and melanoma.⁴ However, most diseases will not show photoacoustic contrast, thereby requiring the use of an exogenous contrast agent that will target the diseased tissue. The main challenge in designing such contrast agent remains creating an agent that produces sufficient photoacoustic signal in order to be detected in low concentration, while being able to target the diseased tissue(s). In this work, we developed a new contrast agent that targets cancer-specific receptor in tumor-bearing mice while producing unprecedented sensitivity.

We have recently reported on the conjugation of cyclic Arg-Gly-Asp (RGD) peptides to pegylated single-walled carbon nanotubes⁵ (SWNT-RGD) and their use as photoacoustic imaging agents⁶ to image $\alpha_v\beta_3$ integrins, which are overexpressed in tumor vasculature. The minimal detectable concentration of SWNT-RGD in living mice was previously

calculated to be ~ 50 nM. In this work, we enhanced the photoacoustic signal of the SWNT-RGD, by attaching Indocyanine Green (ICG) dye to the surface of the nanotubes through π - π stacking interactions⁷ (see Supporting Information for more details). The ultrahigh surface area of the nanotubes allows for highly efficient loading of aromatic molecules such as ICG on the nanotube surface creating a new kind of photoacoustic agent, SWNT-ICG-RGD (Figure 1a). Control untargeted particles were conjugated to a mutated nontargeted peptide, RAD that does not bind to $\alpha_v\beta_3$ integrins.

The optical absorbance spectrum of the new SWNT-ICG nanoparticle reveals that at its peak absorbance at 780 nm the SWNT-ICG particles exhibited a 20-fold higher absorbance as compared with plain SWNTs (Figure 1b). Importantly, SWNT-ICG-RGD had very similar optical spectrum as SWNT-ICG-RAD. We constructed a nonabsorbing and non-scattering agarose phantom with inclusions of SWNT-ICG-RGD at increasing concentrations from 0.5 nM to 121.5 nM in multiples of 3 ($n = 3$ inclusions of each concentration). The photoacoustic signal produced by the SWNT-ICG-RGD particles correlated highly with the nanoparticle concentration ($R^2 = 0.983$) (Figure 1c).

We further validated that the new particles are stable in serum (see Supporting Information and Figure S1). The particle's photobleaching (i.e., loss of optical absorption due to continuous light exposure of the dye component of the

* To whom correspondence should be addressed. E-mail: (S.S.G.) sgambhir@stanford.edu; (H.D.) hdai1@stanford.edu.

† These authors contributed equally to this work.

Received for review: 03/13/2010

Published on Web: 00/00/0000



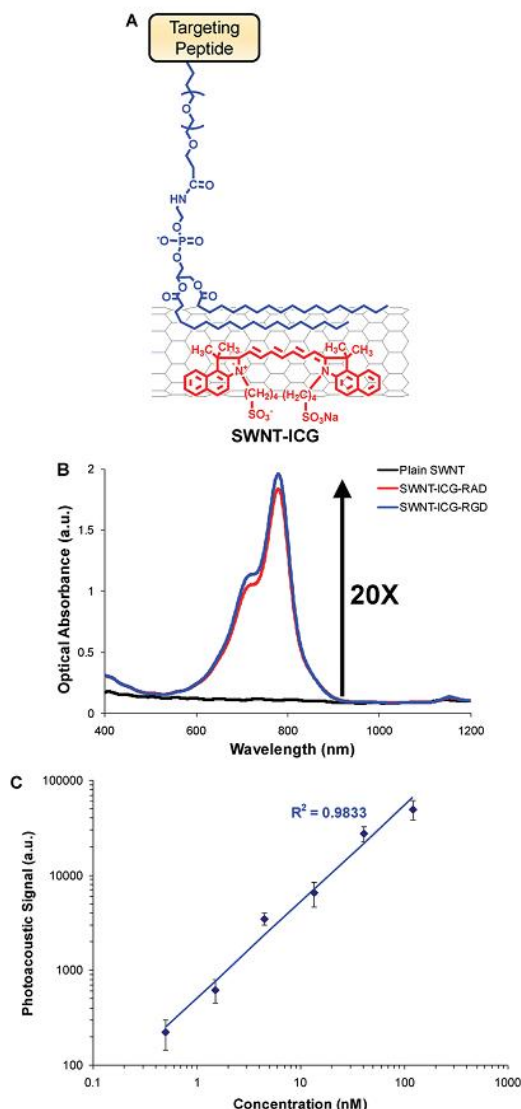


FIGURE 1. Characterization of the ICG dye-enhanced SWNT. (A) Illustration of a SWNT-ICG particle. ICG molecules (red) are attached to the SWNT surface through noncovalent π - π stacking bonds. Polyethylene glycol-5000 (blue) is conjugated to a targeting peptide in one end and to the SWNT surface on the other end through phospholipids. (B) Optical spectra of plain SWNT (black), SWNT-ICG-RGD (blue), and SWNT-ICG-RAD (red). ICG dye-enhanced SWNTs particles showed 20 times higher optical absorption than plain SWNT at the peak absorption wavelength, 780 nm. The similarity of SWNT-ICG-RAD and SWNT-ICG-RGD spectra suggests that the peptide conjugation does not notably perturb the photoacoustic signal. (C) The photoacoustic signal produced by SWNT-ICG was observed to be linearly dependent on the concentration ($R^2 = 0.9833$).

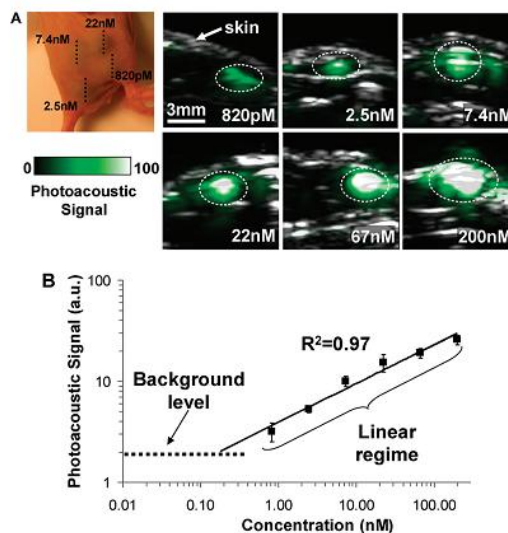


FIGURE 2. Photoacoustic detection of SWNT-ICG in living mice. (A) Mice were injected subcutaneously with SWNT-ICG at concentrations of 0.82–200 nM. The images represent ultrasound (gray) and photoacoustic (green) vertical slices through the subcutaneous injections (dotted black line). The skin is visualized in the ultrasound images, while the photoacoustic images show the SWNT-ICG distribution. The white dotted lines on the images illustrate the approximate edges of each inclusion. (B) The photoacoustic signal from each inclusion was calculated using 3D regions of interest and the “background” represents the endogenous signal measured from tissues. The error bars represent standard error ($n = 3$ mice). Linear regression ($R^2 = 0.97$) of the photoacoustic signal curve estimates that a concentration of 170 pM of SWNT-ICG will give the equivalent background signal of tissues.

nanoparticle) was characterized and found to be relatively small, only 30 % reduction in optical absorption after 60 min of laser irradiation at normal power density of 8 mJ/cm² (see Supporting Information and Figure S2). Finally, cell uptake studies showed specific binding of SWNT-ICG-RGD to U87MG cells compared with the control particles SWNT-ICG-RAD (see Supporting Information and Figure S3).

We then tested the particle’s sensitivity in living subjects by subcutaneously injecting the lower back of mice ($n = 3$) with 30 μ L of SWNT-ICG-RAD mixed with matrigel at increasing concentrations of 820 pM to 200 nM in multiples of 3. Matrigel alone produced no significant photoacoustic signal (data not shown). All animal experiments were performed in compliance with the Guidelines for the Care and Use of Research Animals established by the Stanford University Animal Studies Committee. Upon injection, the matrigel solidified, fixing the SWNT-ICG-RAD in place and three-dimensional (3D) ultrasound and photoacoustic images of the inclusions were acquired (Figure 2a). While the ultrasound image visualized the mouse anatomy (e.g., skin and inclusion edges), the photoacoustic image revealed the SWNT-ICG-RAD contrast in the

mouse. The photoacoustic signal from each inclusion was quantified using a three-dimensional region of interest (ROI) drawn over the inclusion volume. We observed a linear correlation ($R^2 = 0.97$) between the SWNT-ICG-RAD concentration and the corresponding photoacoustic signal (Figure 2b). Tissue background signal was calculated as the average photoacoustic signal in areas where no contrast agent was injected. Extrapolation of the signal-concentration graph reveals that 170 pM of SWNT-ICG-RAD gives the equivalent photoacoustic signal as the tissue background (i.e., signal to background ratio = 1). This value represents over 300 times improvement in sensitivity compared to plain SWNTs.

Finally, we tested the nanoparticles targeting ability in living mice. Mice bearing U87MG tumor xenografts (150 mm³ in size) were injected through the tail vein (IV) with 200 μ L of either SWNT-ICG-RGD (targeted) or SWNT-ICG-RAD (untargeted control) particles ($n = 4$ mice per group) at a concentration of 1.2 μ M. We acquired 3D photoacoustic and ultrasound images of the entire tumor area before and up to 4 h after the injection. Mice injected with SWNT-ICG-RGD showed significantly higher photoacoustic signal in the tumor compared with the control group injected with SWNT-ICG-RAD (Figure 3a). The ultrasound images were used for visualizing the boundaries of the tumor as well as to validate that no significant movement (beyond 100 μ m) had occurred throughout the experiment. While the tumor's photoacoustic signal before the injection is primarily due to the tumor's blood content, the photoacoustic signal postinjection is due to both the blood and the SWNT-ICG particles. To subtract out the background blood signal, a subtraction image calculated as the 2 h postinjection minus the preinjection image was calculated (Figure 3a). Measurement of the photoacoustic signal from a 3D ROI around the tumor (Figure 3b) showed that the photoacoustic signal in the tumor was significantly higher in mice injected with SWNT-ICG-RGD as compared with the control particles SWNT-ICG-RAD ($p < 0.001$). For example, at 2 h postinjection mice injected with SWNT-ICG-RGD showed over 100% higher photoacoustic signal in the tumor than mice injected with the control SWNT-ICG-RAD.

To compare the performance of plain SWNT-RGD to the dye-enhanced SWNT-ICG-RGD, we incubated U87MG cells, which express the target $\alpha_v\beta_3$ on their surface, with either particle solution for 2 h. After incubation, the cells were washed three times with cold saline to remove unbound particles and placed in a clear agarose phantom at increasing concentrations from 25×10^3 to 6×10^6 cells per well ($n = 3$ samples per group) and imaged with the photoacoustic system (Figure 4a). Quantitative analysis of the photoacoustic signal from the phantom revealed that cells exposed to SWNT-ICG-RGD were detected at 20 times lower concentration than cells exposed to plain SWNT-RGD ($p < 0.0001$) (Figure 4a,b). These observations are consistent with the

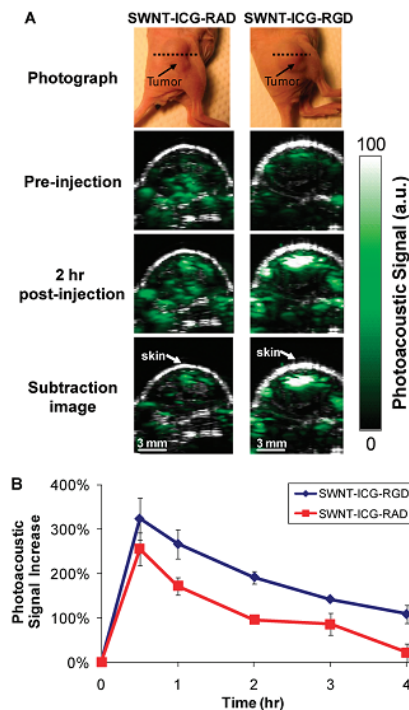


FIGURE 3. SWNT-ICG-RGD tumor targeting in living mice. (A) Ultrasound (gray) and photoacoustic (green) images of one vertical slice through the tumor (dotted black line). The ultrasound images show the skin and the tumor boundaries. Subtraction photoacoustic images were calculated as 2 h postinjection minus preinjection images. As can be seen in the subtraction images, SWNT-ICG-RGD accumulates in higher amount in the tumor as compared to the control SWNT-ICG-RAD. (B) Mice injected with SWNT-ICG-RGD showed significantly higher photoacoustic signal than mice injected with the untargeted control SWNT-ICG-RAD ($p < 0.001$). The error bars represent standard error ($n = 4$ mice).

optical absorbance of SWNT-ICG-RGD being ~ 20 times higher than plain SWNT-RGD.

We have synthesized, characterized, and demonstrated the application of dye-enhanced SWNTs as ultrahigh sensitivity photoacoustic imaging agents. A concentration of 170 pM was estimated to produce an equivalent photoacoustic signal as tissue background signal, representing 300 times improvement in sensitivity as compared with plain SWNTs in living mice. This improvement is likely due to both the higher optical absorption of the particles as well as the fact that the new particle's absorption peak is at 780 nm where the background tissue photoacoustic signal is greatly reduced. Intravenous injection of RGD-targeted SWNT-ICG particles to tumor-bearing mice led to significantly greater accumulation of the particles in the tumor compared to nontargeted control particles. This in vivo targeting study results are likely negatively influenced by the effect of photobleaching, where continued laser light exposure of the

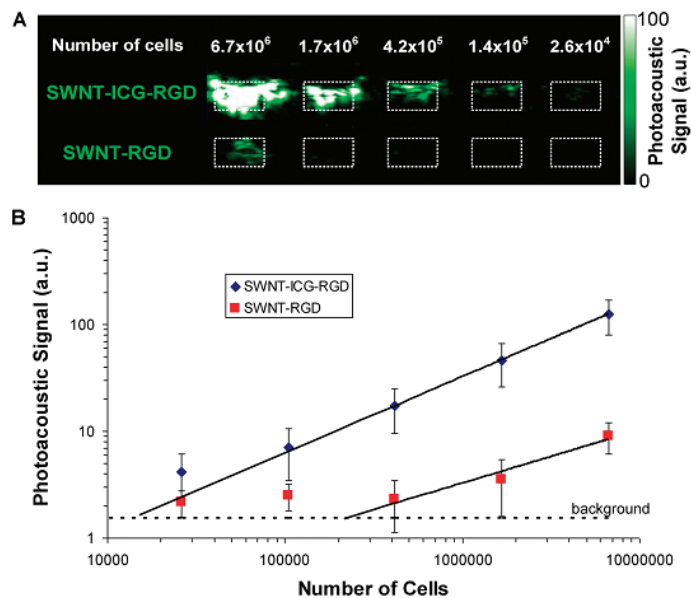


FIGURE 4. Comparison of plain SWNT-RGD to SWNT-ICG-RGD. (A) Photoacoustic vertical slice image through an agarose phantom containing decreasing number of U87 cancer cells exposed to SWNT-ICG-RGD and plain SWNT-RGD particles. While 1.7×10^6 cells exposed to SWNT-RGD are barely seen on the image, a clear photoacoustic signal was observed from 1.4×10^5 cells exposed to SWNT-ICG-RGD. The signal inside the ROI (dotted white boxes) is not homogeneous due to possible aggregates of cells. (B) Quantitative analysis of the photoacoustic signals from the phantom ($n = 3$) showed that SWNT-ICG-RGD can visualize ~ 20 times less cancer cells than SWNT-RGD can ($p < 0.0001$). The background line represents the average background signal in the phantom. Linear regression was calculated on the linear regime of both curves.

tumor caused reduction in the optical absorption (and photoacoustic signal) of the particles that were bound to the tumor. This primarily affects the targeted group, SWNT-ICG-RGD, and to a much lesser extent the untargeted group, SWNT-ICG-RAD, which continued to circulate through the animal's bloodstream unexposed to laser irradiation. Therefore, it is likely that the difference between these two groups is even greater in reality than reflected in the results. Finally, we demonstrated the ability to detect 20 times fewer cancer cells when using SWNT-ICG-RGD as the imaging agent, as compared with plain SWNT-RGD. These results agree with the fact that SWNT-ICG has ~ 20 times greater optical absorbance compared to plain SWNT. Applications of the enhanced particles may therefore be exploited to lead to the earlier detection of cancer by providing the ability to detect smaller tumors.

Most of the work done on photoacoustic contrast agents has been focused on gold nanoparticles^{8–10} as well as other kinds of nanoparticles.^{11,12} However, the main challenge that has yet been solved is the delivery of such agents to the tumor in sufficient amounts to create detectable and specific signal. This is likely due to the particles' large size that leads to rapid clearance by the reticuloendothelial system (RES) upon intravenous injection, preventing the particles from accumulating at the tumor site. In contrast, the SWNTs used

here are 1–2 nm in diameter and 50–300 nm in length. Since the dye we used was attached to the surface of the SWNTs under the PEG, it is expected that the total particle size was not significantly changed, thereby allowing the particles to keep a favorable biodistribution as previously reported.⁵ Hence, the dye-enhanced SWNTs presented in this work offer unprecedented photoacoustic signal strengths while maintaining relatively small size allowing them to target tumors upon intravenous injection. We have also previously published pilot toxicology studies of the SWNTs with encouraging results in mouse models¹³ as well as observed they are able to be excreted via the biliary pathway.¹⁴

The reason for loading a SWNT with many small ICG dye molecules is the high efficiency of optical absorption of ICG dye compared to its weight. According to the parameter of optical absorption divided by weight, ICG is 7 times more efficient than SWNTs and ~ 8500 times more efficient than commercial gold nanorods with a peak absorption at 780 nm.

The dye-enhanced SWNT photoacoustic contrast agents reported here have the capability to bind to molecular targets in living animals while maintaining a very high photoacoustic signal. No other imaging modality or imaging agent can achieve sub-nM sensitivity at large depths of penetration and



submillimeter spatial resolution as can be achieved with photoacoustic imaging of dye-enhanced SWNTs.

Acknowledgment. We would like to acknowledge funding from the National Institute of Health (NIH) grants NCI CCNE U54 CA119367 (SSG), NCI ICMIC P50 CA114747 (SSG), and the Canary Foundation for supporting this work. A.D. is partially funded from the Bio-X Graduate Student Fellowship and the DoD Breast Cancer Research Program — Predoctoral Traineeship Award. The authors would also like to thank J. Rosenberg for the statistical analysis and Omer Oralkan and Te-Jen Ma for useful discussions.

Supporting Information Available. Description of particles synthesis, photoacoustic imaging instrument, experimental procedures, statistical methods, and in vitro characterization of the particles including serum-stability, photobleaching, and cell-uptake study. This material is available free of charge via the Internet at <http://pubs.acs.org>.

REFERENCES AND NOTES

- (1) Xu, M. H.; Wang, L. H. V. *Rev. Sci. Instrum.* **2006**, *77* (4), No. 041101–043100.
- (2) Maslov, K.; Zhang, H. F.; Hu, S.; Wang, L. V. *Opt. Lett.* **2008**, *33* (9), 929–31.
- (3) Zhang, H. F.; Maslov, K.; Stoica, G.; Wang, L. V. *J. Biomed. Opt.* **2006**, *11* (5), No. 054033.
- (4) Zhang, H. F.; Maslov, K.; Stoica, G.; Wang, L. V. *Nat. Biotechnol.* **2006**, *24* (7), 848–51.
- (5) Liu, Z.; Cai, W.; He, L.; Nakayama, N.; Chen, K.; Sun, X.; Chen, X.; Dai, H. *Nat. Nanotechnol.* **2007**, *2* (1), 47–52.
- (6) de la Zerde, A.; Zavaleta, C.; Keren, S.; Vaithilingam, S.; Bodapati, S.; Liu, Z.; Levi, J.; Smith, B. R.; Ma, T. J.; Oralkan, O.; Cheng, Z.; Chen, X.; Dai, H.; Khuri-Yakub, B. T.; Gambhir, S. S. *Nat. Nanotechnol.* **2008**, *3* (9), 557–62.
- (7) Liu, Z.; Sun, X.; Nakayama-Ratchford, N.; Dai, H. *ACS Nano* **2007**, *1* (1), 50–56.
- (8) Kim, J. W.; Galanzha, E. I.; Shashkov, E. V.; Moon, H. M.; Zharov, V. P. *Nat. Nanotechnol.* **2009**, *4* (10), 688–94.
- (9) Eghtedari, M.; Oraevsky, A.; Copland, J. A.; Kotov, N. A.; Conjusteau, A.; Motamedi, M. *Nano Lett.* **2007**, *7* (7), 1914–8.
- (10) Yang, X.; Skrabalak, S. E.; Li, Z. Y.; Xia, Y.; Wang, L. V. *Nano Lett.* **2007**, *7* (12), 3798–802.
- (11) Kim, G.; Huang, S. W.; Day, K. C.; O'Donnell, M.; Agayan, R. R.; Day, M. A.; Kopelman, R.; Ashkenazi, S. *J. Biomed. Opt.* **2007**, *12* (4), No. 044020.
- (12) Zhang, Q.; Iwakuma, N.; Sharma, P.; Moudgil, B. M.; Wu, C.; McNeill, J.; Jiang, H.; Grobmyer, S. R. *Nanotechnology* **2009**, *20* (39), 395102.
- (13) Schipper, M. L.; Nakayama-Ratchford, N.; Davis, C. R.; Kam, N. W. S.; Chu, P.; Liu, Z.; Sun, X.; Dai, H.; Gambhir, S. S. *Nat. Nanotechnol.* **2008**, *3* (4), 216–221.
- (14) Liu, Z.; Davis, C.; Cai, W.; He, L.; Chen, X.; Dai, H. *Proc. Natl. Acad. Sci. U.S.A.* **2008**, *105* (5), 1410–5.



Family of Enhanced Photoacoustic Imaging Agents for High Sensitivity and Multiplexing Studies in Living Mice

*Adam de la Zerda^{1,2}, Sunil Bodapati¹, Robert Teed¹, Salomon Y. May¹,
Scott M. Tabakman³, Zhuang Liu^{3,4}, Butrus T. Khuri-Yakub², Xiaoyuan Chen^{1,5},
Hongjie Dai³, Sanjiv Sam Gambhir^{1,6}*

¹Molecular Imaging Program at Stanford, Department of Radiology and Bio-X Program, the

²Department of Electrical Engineering and the ³Department of Chemistry, Stanford University, Palo Alto, CA 94305, USA, ⁴Institute of Functional Nano & Soft Materials (FUNSOM), Soochow University, Suzhou, Jiangsu, 215123, China, ⁵Laboratory for Molecular Imaging and Nanomedicine, National Institute of Biomedical Imaging and Bioengineering (NIBIB), National Institutes of Health (NIH), Bethesda, MD 20892, USA, ⁶Department of Bioengineering, Department of Materials Science & Engineering, Stanford University, Palo Alto, CA 94305, USA.

* e-mail: sgambhir@stanford.edu

Abstract

Photoacoustic imaging is an emerging modality that overcomes to a great extent the resolution and depth limitations of optical imaging while maintaining relatively high-contrast. However, since many diseases will not manifest an endogenous photoacoustic contrast, it is essential to develop exogenous photoacoustic contrast agents that can target diseased tissue(s). Here we present a family of novel photoacoustic contrast agents that are based on the binding of small optical dyes to single walled carbon nanotubes (SWNT-dye). We synthesized five different SWNT-dye contrast agents using different optical dyes, creating five “flavors” of SWNT-dye nanoparticles. In particular, SWNT that were coated with either QSY₂₁ (SWNT-QSY) or Indocyanine Green (SWNT-ICG) exhibited over 100-times higher photoacoustic contrast in living animals compared to plain SWNTs, leading to subnanomolar sensitivities. We then conjugated the SWNT-QSY and SWNT-ICG particles with cyclic Arg-Gly-Asp (RGD) peptides to molecularly target the $\alpha_v\beta_3$ integrin, which is associated with tumor angiogenesis. Intravenous administration of these tumor-targeted imaging agents to tumor-bearing mice showed significantly higher photoacoustic signal in the tumor than in mice injected with the untargeted contrast agent. Finally, we were able to spectrally separate the photoacoustic signals of SWNT-QSY and SWNT-ICG in living animals injected subcutaneously with both particles in the same location, opening the possibility for multiplexing in-vivo studies.

Introduction

Photoacoustic molecular imaging is an emerging imaging modality where disease-targeted imaging agents produce ultrasound waves in response to the absorption of short-pulsed laser light¹⁻⁴. The main advantage of the photoacoustic imaging modality is in its higher depth of penetration and spatial resolution, as compared with purely optical techniques. However, the main challenge in designing photoacoustic imaging agents is creating an agent that produces sufficient photoacoustic signal in order to be detected in low concentration, while being able to target the diseased tissue(s). Moreover, it is desirable to have multiple imaging agents, each with a different optical spectrum so to allow multiplexing studies. In this work, we report on a general method to prepare a dye-enhanced single walled carbon nanotubes (SWNTs) photoacoustic imaging agents by coating small molecule dyes onto the surface of SWNTs. We show that the resulting imaging agents can target cancer-specific receptors in tumor-bearing mice, exhibit unprecedented high sensitivity and can be imaged simultaneously (multiplexed).

Results

We have recently reported on the conjugation of cyclic Arg-Gly-Asp (RGD) peptides to pegylated SWNTs⁵ (SWNT-RGD) and their use as photoacoustic imaging agents¹ to image $\alpha_v\beta_3$ integrins, which are over-expressed in tumor vasculature. We then also reported on the binding of Indocyanine Green (ICG) to the surface of the SWNTs through pi-pi stacking⁶. This loading of ICG onto the surface of the SWNTs has resulted in significantly better in-vivo sensitivity than plain SWNTs. In this work we generalize this method and show it works for a number of optical dyes and quenchers including QSY₂₁, Methylene Blue (MB), Cyanine dyes such as Cy5.5, and Melanin (**Fig. 1a**). Control untargeted SWNT-dye particles were conjugated to a mutated non-targeted peptide, RAD that does not bind to $\alpha_v\beta_3$ integrins (see **Supporting Information** for more details on syntheses).

The ultra-high surface area to volume ratio of the nanotubes allowed for efficient loading of the optical dyes onto the nanotubes. The SWNT-dye conjugates exhibited a significant increase in the optical absorption compared to plain SWNTs to the extent of 120%, 88% and 30% increase for Methylene Blue, Cy5.5 and Melanin respectively (**Fig. 1b**). Of most interest were ICG and QSY₂₁ dyes whose conjugates with SWNTs led to 20 and 17-fold increase in the particles' optical absorption respectively (**Fig. 1c**). Furthermore, the spectra of SWNT-ICG and SWNT-QSY peak at different wavelengths; 710 nm and 780 nm respectively. We therefore selected SWNT-ICG and SWNT-QSY as the candidate molecular imaging agents to demonstrate multiplexing in this work. Importantly, the nanoparticles conjugated with RAD and RGD had

nearly identical absorption spectra (see **Supporting Information** and **Supplementary Fig. S1**), suggesting that the peptide conjugation did not interfere with the particle's photoacoustic signal.

We constructed a non-absorbing and non-scattering agarose phantom with inclusions of SWNT-QSY-RGD and SWNT-ICG-RGD and at increasing concentrations from 0.5 nM to 121.5 nM in multiples of 3 ($n = 3$ inclusions per concentration). We used our home-made photoacoustic imaging system (see **Supporting Information** and **Supplementary Fig. S5**) and scanned the phantom at 710 nm and 780 nm for the QSY- and ICG-coated particles respectively. The photoacoustic signal produced by the SWNT-QSY-RGD and SWNT-ICG-RGD particles correlated highly with the nanoparticle concentration ($R^2 = 0.99$ and 0.98 respectively) (**Fig. 1c**).

We further validated that the new particles are stable in serum (see **Supporting Information** and **Supplementary Fig. S2**). The particle's photobleaching (i.e., loss of optical absorption due to continuous light exposure of the dye component of the nanoparticle) was characterized and found to be relatively small for SWNT-ICG, only 30% reduction in optical absorption after 60 min of laser irradiation at normal power density of 8 mJ/cm^2 . SWNT-QSY, however, showed higher light-sensitivity, resulting in a 50% reduction in optical absorption after 7 min of laser irradiation (see **Supporting Information** and **Supplementary Fig. S3**). Finally, cell uptake studies showed specific binding of SWNT-QSY-RGD and SWNT-ICG-RGD to U87MG cells compared with the control particles SWNT-QSY-RAD and SWNT-ICG-RAD respectively (see **Supporting Information** and **Supplementary Fig. S4**).

We then tested the particle's sensitivity in living subjects by subcutaneously injecting the lower back of mice ($n = 3$) with $30 \text{ } \mu\text{l}$ of SWNT-QSY-RGD or SWNT-ICG-RGD mixed with matrigel at increasing concentrations between 500 pM to 200 nM. Matrigel alone produced no significant photoacoustic signal (data not shown). All animal experiments were performed in compliance with the Guidelines for the Care and Use of Research Animals established by the Stanford University Animal Studies Committee. Upon injection, the matrigel solidified, fixing the nanoparticles in place and three-dimensional (3D) ultrasound and photoacoustic images of the inclusions were acquired (**Fig. 2a**). While the ultrasound image visualized the mouse anatomy (e.g., skin and inclusion edges), the photoacoustic image revealed the nanoparticles' contrast in the mouse tissue. The photoacoustic signal from each inclusion was quantified using a three dimensional region of interest (ROI) drawn over the inclusion volume. We observed a linear correlation ($R^2 = 0.97$ for both particles) between the nanoparticles concentration and the corresponding photoacoustic signal (**Fig. 2b**). Tissue background signal was calculated as the average photoacoustic signal in areas where no nanoparticles were injected. Extrapolation of the

signal-concentration graph reveals that 450 pM of SWNT-QSY-RGD and 170 pM of SWNT-ICG-RGD give the equivalent photoacoustic signal as the tissue background (i.e., signal to background ratio = 1). This value represents over 100-times improvement in sensitivity compared to plain SWNTs.

We then tested the nanoparticles targeting ability in living mice. Mice bearing U87MG tumor xenografts (150 mm³ in size) were injected through the tail vein (IV) with 200 µl of either SWNT-QSY-RGD (targeted) or SWNT-QSY-RAD (untargeted control) or the ICG-particles (n = 3 mice per group) at a concentration of 1.2 µM. We acquired 3D photoacoustic and ultrasound images of the entire tumor area before and 2 hours after the injection. Mice injected with the RGD-targeted nanoparticles showed significantly higher photoacoustic signal in the tumor compared with the control group injected with the RAD control particles (**Fig. 3a**). The ultrasound images were used for visualizing the boundaries of the tumor as well as to validate that no significant movement (beyond 100 µm) had occurred throughout the experiment. While the tumor's photoacoustic signal before the injection is primarily due to the tumor's blood content, the photoacoustic signal post-injection is due to both the blood and the nanoparticles. To subtract out the background blood signal, subtraction images were calculated as the post-injection minus the pre-injection images, leaving the image only with the contrast made by the nanoparticles (**Fig. 3a**). Measurement of the photoacoustic signal from a 3D ROI around the tumor (**Fig. 3b**) showed that the photoacoustic signal in the tumor was significantly higher in mice injected with the RGD-targeted nanoparticles as compared with the control particles ($p < 0.01$ for both QSY and ICG nanoparticles). For example, at 2 hours post-injection, mice injected with SWNT-QSY-RGD showed over 3-times higher photoacoustic signal increase in the tumor than mice injected with the control SWNT-QSY-RAD.

While the optical absorption spectra of SWNT-QSY and SWNT-ICG overlap, they are not identical, opening the possibility to spectrally unmix their signals, even at situations where they are spatially co-localized. We prepared an optically clear agarose-based phantom where in each of 5 wells, SWNT-QSY and SWNT-ICG were mixed in various ratios (pure SWNT-ICG, 1:3, 1:1, 3:1 and pure SWNT-QSY). Photoacoustic images at 700, 730, 760, 780, 800 nm were taken (**Fig. 4a**) and used in a least squares method (see Supplementary Information for more details) to unmix the photoacoustic signals produced by the SWNT-QSY and the SWNT-ICG particles (**Fig. 4b**).

Finally, we injected 30 µl of an equal mixture of SWNT-QSY and SWNT-ICG at 50 nM subcutaneously to a living mouse flank (**Fig. 5a**). Control injections of 30 µl of SWNT-QSY and SWNT-ICG alone were injected subcutaneously to the mouse flank as well. Photoacoustic

images at 700, 730, 760, 780, 800 nm (**Fig. 5e**) were used to spectrally unmix the SWNT-QSY and the SWNT-ICG signals. Indeed, the SWNT-QSY injection site showed only SWNT-QSY signal (**Fig. 5b**), the SWNT-ICG injection site showed primarily SWNT-ICG signal (**Fig. 5c**), while the site that was injected with the equal mixture of particles showed both SWNT-QSY and SWNT-ICG signal (**Fig. 5d**). At the area of injection, a slight separation of photoacoustic signals of the two channels (SWNT-QSY and SWNT-ICG) was observed. These image reconstruction artifacts are likely caused by slight movements of the mouse between the acquisition of consecutive photoacoustic images at different wavelengths, as well as differences in light tissue distribution between the five wavelengths.

Discussion

We have synthesized, characterized and demonstrated the application of dye-enhanced SWNTs as ultra-high sensitivity photoacoustic imaging agents. Concentrations of 170 pM and 450 pM were estimated to be the in-vivo sensitivity limits for the two nanoparticles, representing over 100-times improvement over plain SWNTs¹ and nearly 3-fold higher sensitivity than can be achieved using fluorescence imaging of quantum dots in living mice⁷. This improvement is likely due to both the higher optical absorption of the particles as well as the fact that the new particle's absorption peak is further red-shifted than plain SWNTs where the background tissue photoacoustic signal is greatly reduced. Most importantly, intravenous injection of RGD-targeted SWNT-QSY and SWNT-ICG particles to tumor-bearing mice led to significantly greater accumulation of the particles in the tumors compared to non-targeted control particles. Despite the fact that plain SWNT-RGD were able to target tumors in living mice, it could not have been predicted that SWNT-dye-RGD would also target tumors in living mice. This is because the extra dye-coating may increase the size and molecular weight of the particles and may even change its surface charge and zeta-potential. Finally, we demonstrated the ability to multiplex the signals from SWNT-QSY and SWNT-ICG both in-vitro as well as in living mice. Applications of the enhanced particles may therefore be exploited to lead to the earlier detection of cancer by providing the ability to detect smaller tumors and likely provide molecular information on multiple targets.

While small optical dyes have lower optical absorption, they are also significantly smaller than nanoparticles. For example, ICG absorption coefficient divided by its molecular weight is still 7-times greater than that of a plain SWNT, or 9000-times greater than a gold nanorod with peak absorption at 780 nm. This suggests that creating a carrier for small optical dyes, such as SWNT, may be highly beneficial, as indeed shown in this work.

Photoacoustic imaging has been primarily used to visualize endogenous absorbers (e.g., hemoglobin and melanin) in the body⁸⁻¹¹. However, in order to visualize molecular characteristics of a tumor, an exogenous contrast agent that is specific for a given molecular target is required. Most work on photoacoustic contrast agents has been focused on gold nanoparticles¹²⁻¹⁶ as well as other kinds of nanoparticles¹⁷⁻¹⁹ and small molecules²⁰. However, the main challenge that has yet been solved is the delivery of such agents to the tumor in sufficient amounts to create detectable and specific signal. High and rapid uptake of the nanoparticles by the reticuloendothelial system (RES) is likely the cause preventing the particles from accumulating at the tumor site in sufficient amounts. The SWNTs used here are 1-2 nm in diameter and 50-300 nm in length. It is believed that this size is maintained even after the conjugation of the small optical dyes to the SWNT surface, as the dyes are conjugated directly to the surface of the nanotube, under the polyethylene-glycol (PEG), thereby allowing the particles to keep a favorable bio-distribution as reported previously⁵. Hence, the dye-enhanced SWNTs presented in this work offer both unprecedented photoacoustic sensitivity as well as good tumors targeting capabilities upon intravenous injection. We have also previously published pilot toxicology studies of the SWNTs with encouraging results in mouse models²¹ as well as observed they are able to be excreted via the biliary pathway^{22, 23}.

The dye-enhanced SWNT photoacoustic contrast agents reported here have the capability to bind to molecular targets in living animals while maintaining a very high photoacoustic signal and present multiplexing capabilities. No other imaging modality or imaging agent can achieve both sub-nM sensitivity at large depths of penetration and sub-millimeter spatial resolution as can be achieved with photoacoustic imaging of dye-enhanced SWNTs. To our knowledge, this is the first demonstration of multiplexing of photoacoustic molecular imaging agents that are capable to molecularly target tumors in living animals.

Supporting Information

Description of particles synthesis, photoacoustic imaging instrument, experimental procedures, statistical methods, and in-vitro characterization of the particles including serum-stability, photobleaching and cell-uptake study.

References

1. de la Zerda, A.; Zavaleta, C.; Keren, S.; Vaithilingam, S.; Bodapati, S.; Liu, Z.; Levi, J.; Smith, B. R.; Ma, T. J.; Oralkan, O.; Cheng, Z.; Chen, X.; Dai, H.; Khuri-Yakub, B. T.; Gambhir, S. S. *Nat Nanotechnol* **2008**, 3, (9), 557-62.
2. Wang, L. V. *Nat Photon* **2009**, 3, (9), 503-509.
3. Razansky, D.; Distel, M.; Vinegoni, C.; Ma, R.; Perrimon, N.; Koster, R. W.; Ntziachristos, V. *Nat Photon* **2009**, 3, (7), 412-417.
4. Ntziachristos, V.; Razansky, D. *Chem Rev* **2010**, 110, (5), 2783-94.
5. Liu, Z.; Cai, W.; He, L.; Nakayama, N.; Chen, K.; Sun, X.; Chen, X.; Dai, H. *Nat Nanotechnol* **2007**, 2, (1), 47-52.
6. de la Zerda, A.; Liu, Z.; Bodapati, S.; Teed, R.; Vaithilingam, S.; Khuri-Yakub, B. T.; Chen, X.; Dai, H.; Gambhir, S. S. *Nano Lett* **2010**, 10, (6), 2168-72.
7. de la Zerda, A.; Bodapati, S.; Teed, R.; Schipper, M.; Keren, S.; Smith, B.; Ng, J.; Gambhir, S. S. *Molecular Imaging and Biology* **2009**.
8. Zhang, H. F.; Maslov, K.; Stoica, G.; Wang, L. V. *Nat Biotechnol* **2006**, 24, (7), 848-51.
9. Oh, J. T.; Li, M. L.; Zhang, H. F.; Maslov, K.; Stoica, G.; Wang, L. V. *J Biomed Opt* **2006**, 11, (3), 034032.
10. de la Zerda, A.; Paulus, Y. M.; Teed, R.; Bodapati, S.; Dollberg, Y.; Khuri-Yakub, B. T.; Blumenkranz, M. S.; Moshfeghi, D. M.; Gambhir, S. S. *Opt Lett* **2010**, 35, (3), 270-2.
11. Laufer, J.; Zhang, E.; Raivich, G.; Beard, P. *Appl Opt* **2009**, 48, (10), D299-306.
12. Mallidi, S.; Larson, T.; Tam, J.; Joshi, P. P.; Karpouk, A.; Sokolov, K.; Emelianov, S. *Nano Lett* **2009**, 9, (8), 2825-31.
13. Kim, J. W.; Galanzha, E. I.; Shashkov, E. V.; Moon, H. M.; Zharov, V. P. *Nat Nanotechnol* **2009**, 4, (10), 688-94.
14. Eghtedari, M.; Oraevsky, A.; Copland, J. A.; Kotov, N. A.; Conjusteau, A.; Motamedi, M. *Nano Letters* **2007**, 7, (7), 1914-8.
15. Yang, X.; Skrabalak, S. E.; Li, Z. Y.; Xia, Y.; Wang, L. V. *Nano Lett* **2007**, 7, (12), 3798-802.
16. Agarwal, A.; Huang, S. W.; O'Donnell, M.; Day, K. C.; Day, M.; Kotov, N.; Ashkenazi, S. *Journal of Applied Physics* **2007**, 102, (6), 064701-4.
17. Kim, G.; Huang, S. W.; Day, K. C.; O'Donnell, M.; Agayan, R. R.; Day, M. A.; Kopelman, R.; Ashkenazi, S. *J Biomed Opt* **2007**, 12, (4), 044020.
18. Zhang, Q.; Iwakuma, N.; Sharma, P.; Moudgil, B. M.; Wu, C.; McNeill, J.; Jiang, H.; Grobmyer, S. R. *Nanotechnology* **2009**, 20, (39), 395102.
19. Bouchard, L. S.; Anwar, M. S.; Liu, G. L.; Hann, B.; Xie, Z. H.; Gray, J. W.; Wang, X.; Pines, A.; Chen, F. F. *Proc Natl Acad Sci U S A* **2009**, 106, (11), 4085-9.
20. Levi, J.; Kothapalli, S. R.; Ma, T. J.; Hartman, K.; Khuri-Yakub, B. T.; Gambhir, S. S. *J Am Chem Soc* **2010**, 132, (32), 11264-9.
21. Schipper, M. L.; Nakayama-Ratchford, N.; Davis, C. R.; Kam, N. W. S.; Chu, P.; Liu, Z.; Sun, X.; Dai, H.; Gambhir, S. S. *Nat Nano* **2008**, 3, (4), 216-221.
22. Liu, Z.; Davis, C.; Cai, W.; He, L.; Chen, X.; Dai, H. *Proc Natl Acad Sci U S A* **2008**, 105, (5), 1410-5.
23. Liu, Z.; Tabakman, S.; Welsher, K.; Dai, H. *Nano Research* **2009**, 2, (2), 85-120.

Acknowledgments

We would like to acknowledge funding from the National Institute of Health (NIH) grants NCI CCNE U54 CA119367 (SSG), NCI ICMIC P50 CA114747 (SSG), and the Canary Foundation

for supporting this work. A. de la Zerda is partially funded from the Bio-X Graduate Student Fellowship and the DoD Breast Cancer Research Program – Pre-doctoral Traineeship Award. The authors would also like to thank Srikant Vaithilingam, Omer Oralkan and Te-Jen Ma for useful discussions.

Figures:

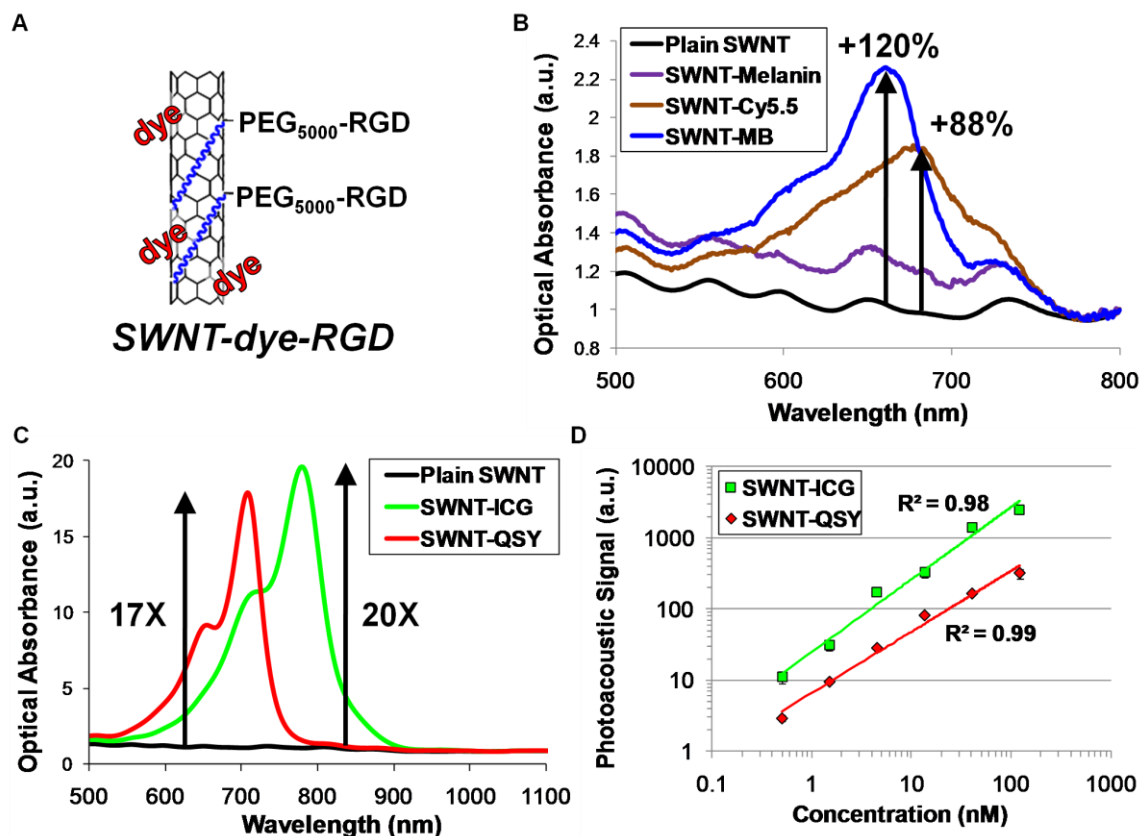


Figure 1. Characterization of the dye-enhanced SWNT. (A) Illustration of a SWNT-QSY and SWNT-ICG particle. QSY₂₁ and ICG molecules (red) are attached to the SWNT surface through non-covalent pi-pi stacking bonds. Polyethylene glycol-5000 (blue) is conjugated to a targeting peptide in one end and to the SWNT surface on the other end through phospholipids. (B) Optical spectra of plain SWNT (black), SWNT-QSY-RGD (red) and SWNT-ICG-RGD (green). QSY and ICG dye-enhanced SWNTs particles showed 17 and 20-times higher optical absorption than plain SWNT at the peak absorption wavelength, 710 and 780 nm respectively. (C) The photoacoustic signal produced by SWNT-QSY and SWNT-ICG was observed to be linearly dependent on the particles' concentration ($R^2 = 0.99$ and 0.98 respectively).

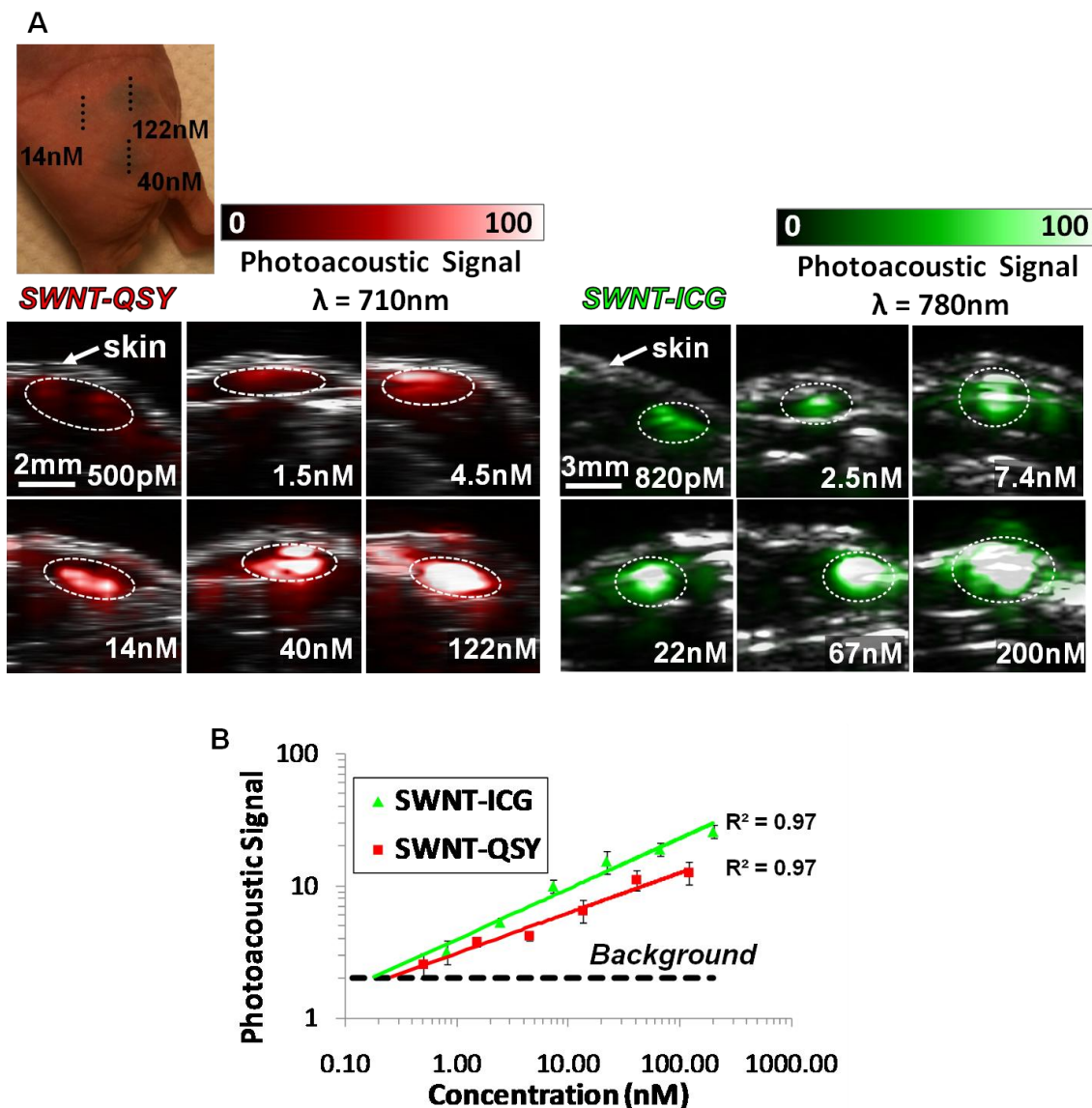


Figure 2. Photoacoustic detection of dye-SWNT particles in living mice. (A) Mice were injected subcutaneously with SWNT-QSY or SWNT-ICG at concentrations between 0.5-200 nM. The images represent ultrasound (gray), photoacoustic image acquired at $\lambda = 710$ nm (red) and photoacoustic image acquired at $\lambda = 780$ nm (green) vertical slices through the subcutaneous injections (dotted black line on the mouse picture). The skin and inclusion volume are visualized in the ultrasound images, while the photoacoustic images visualize the nanoparticles contrast agents. The white dotted lines on the images illustrate the approximate edges of each inclusion. (B) The photoacoustic signal from each inclusion was calculated using 3D regions of interest and the „background’ represents the endogenous signal measured from tissues. The error bars represent standard error ($n = 3$ mice). Linear regression ($R^2 = 0.97$ for both particles) of the photoacoustic signal curves estimates that a concentration of 450 pM of SWNT-QSY or 170 pM of SWNT-ICG will give the equivalent background signal of tissues.

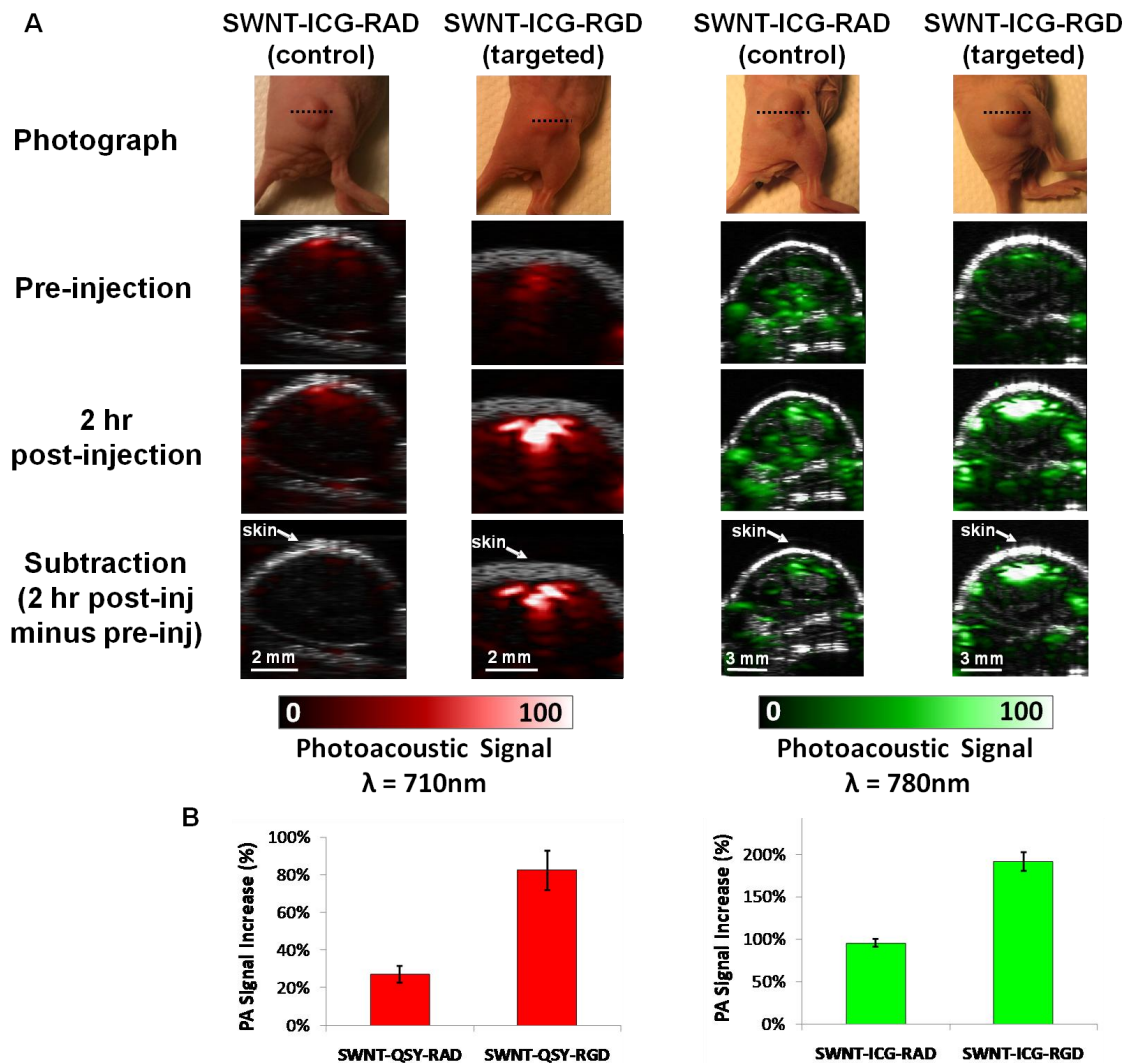


Figure 3. Dye-SWNT tumor targeting in living mice. (A) Ultrasound (gray) and photoacoustic (red for $\lambda = 710$ nm and green for $\lambda = 780$ nm) images of a vertical slice through the tumors (dotted black line). The ultrasound images show the skin and the tumor boundaries. Subtraction photoacoustic images were calculated as 2 hr post-injection minus pre-injection images. As can be seen in the subtraction images, SWNT-QSY-RGD as well as SWNT-ICG-RGD accumulate in significantly higher amounts in the tumor as compared to their respective control particles. (B) Quantitative region-of-interest analysis shows that SWNT-QSY-RGD creates a 3-fold higher photoacoustic signal increase in the tumor than the control SWNT-QSY-RAD particle ($p < 0.01$). SWNT-ICG-RGD provides over 100% higher photoacoustic signal increase than the control SWNT-ICG-RAD ($p < 0.01$). The error bars represent standard error ($n = 3$ mice)

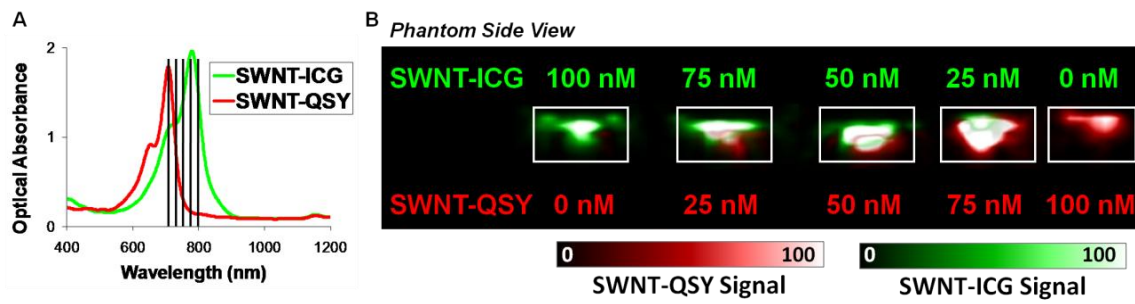


Figure 4. Multiplexing of SWNT-QSY with SWNT-ICG *in-vitro*. (A) An agarose phantom containing SWNT-ICG and SWNT-QSY at different mixture concentrations (pure SWNT-ICG, 1:3, 1:1, 3:1 and pure SWNT-QSY) was scanned using the photoacoustic instrument at 5 different wavelengths (at 700, 730, 760, 780, 800 nm). (B) Despite their overlapping spectra, the photoacoustic signals from SWNT-QSY and SWNT-ICG were unmixed.

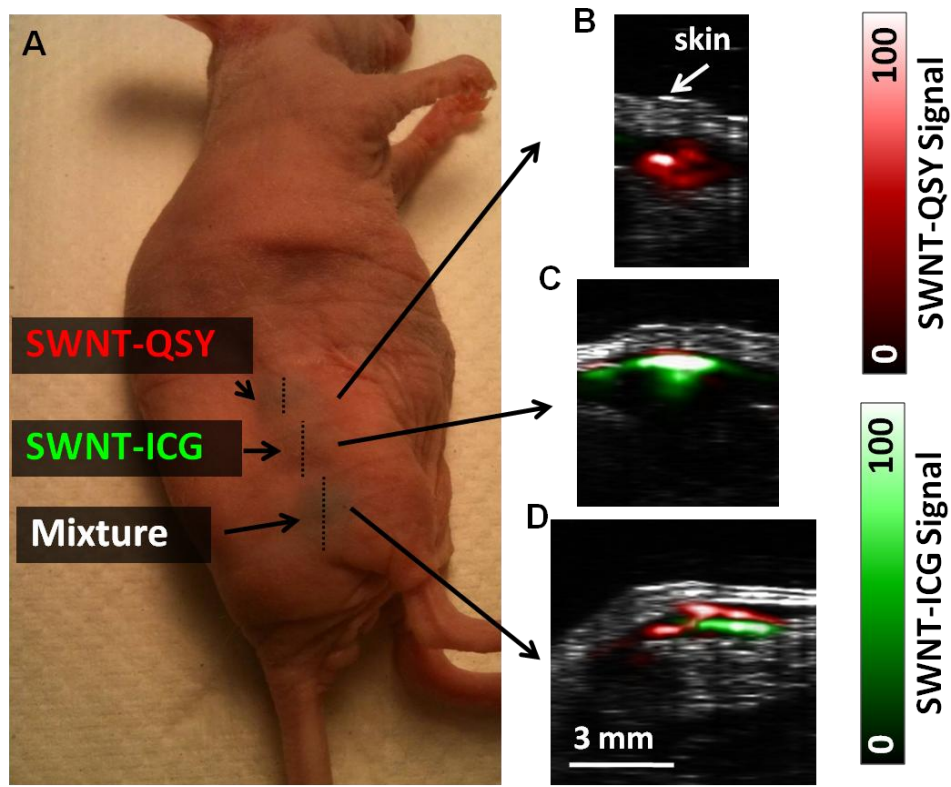


Figure 5. Multiplexing of SWNT-QSY with SWNT-ICG in living mice. (A) Mouse injected with 30 μ l of 50 nM SWNT-QSY (upper inclusion), 30 μ l of 50 nM SWNT-ICG (middle inclusion) and 30 μ l of an equal mixture of 50 nM of SWNT-QSY and SWNT-ICG (lower inclusion). (B) The unmixed photoacoustic vertical slice through the upper inclusion, showing only red signal from the SWNT-QSY. (C) The unmixed photoacoustic slice through the middle inclusion, showing mostly green signal from the SWNT-ICG. (D) The unmixed photoacoustic slice through the lower inclusion, showing both red and green signals of SWNT-QSY and SWNT-ICG spread throughout the inclusion area. Image reconstruction artifacts as well as

inhomogeneous light penetration into the tissue are likely the cause for the separation of the green and red signals in the image. **(E)** The wavelengths used for the photoacoustic scans were 700, 730, 760, 780, 800 nm.

3. Abstract presented at World Molecular Imaging Congress 2010:

Family of enhanced photoacoustic imaging agents for high sensitivity and multiplexing studies in living mice

Adam de la Zerda, Sunil Bodapati, Robert M. Teed, Scott Tabakman, Zhuang Liu, Butrus T. Khuri-Yakub, Xiaoyuan Chen, Hongjie Dai, Sanjiv Sam Gambhir

Photoacoustic molecular imaging of living subjects offers high spatial resolution at increased tissue depths compared to optical imaging. We have recently shown that intravenously injected single walled carbon nanotubes (SWNTs) can be used as targeted photoacoustic imaging agents in living mice.

We have synthesized two new photoacoustic imaging agents based on SWNT conjugated to either QSY₂₁ (SWNT-QSY) or to Indocyanine Green (SWNT-ICG) through strong pi-pi stacking interactions with the nanotubes. The particles were conjugated to cyclic Arg-Gly-Asp (RGD) peptides to molecularly target the $\alpha_v\beta_3$ integrins, which are associated with tumor angiogenesis. Control particles were conjugated to the RAD peptide (which does not bind to $\alpha_v\beta_3$).

We verified both particles are stable in serum and can target $\alpha_v\beta_3$ integrin through cell uptake studies with U87 cells. We found the photoacoustic signal to be highly linear to the particles' concentration both in phantom studies ($R^2 = 0.99$, $R^2 = 0.98$) as well as in living mice injected subcutaneously with the particles ($R^2 = 0.96$, $R^2 = 0.97$ for SWNT-QSY and SWNT-ICG respectively). We measured the detection sensitivity of SWNT-QSY and SWNT-ICG in living mice ($n = 3$) to be 450 pM and 170 pM respectively, which represents 110-fold and 300-fold improvement compared to plain SWNTs respectively ($p < 0.05$).

U87 tumor-bearing mice were injected via the tail-vein with RGD-targeted SWNT-QSY or SWNT-ICG. At 2 hours post-injection, mice injected with the RGD-targeted particles showed significantly higher photoacoustic signal in the tumor compared to mice injected with the control RAD-labeled particles ($p < 0.05$ for both particles, $n = 4$ per group).

While overlapping, the optical absorption spectra of SWNT-QSY and SWNT-ICG are different, which allowed us to spectrally separate their photoacoustic signals both in a phantom as well as in living mice (see **Figure**).

This is the first demonstration of true multiplexing of photoacoustic imaging agents that were also shown to target tumors in living mice.

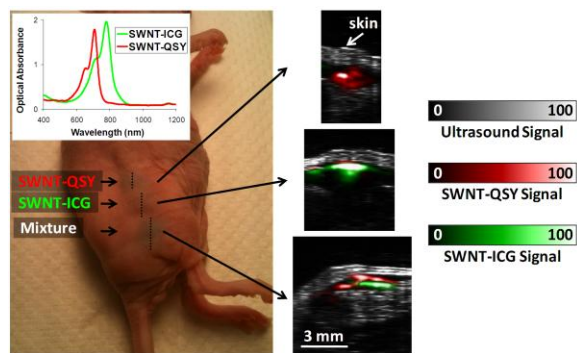


Figure: SWNT-QSY (red) and SWNT-ICG (green) were multiplexed in subcutaneous injections in living mice with our photoacoustic instrument, despite their overlapping spectra.

4. Abstract submitted to Era of Hope 2011:

Photoacoustic Molecular Imaging using Carbon Nanotubes for Ultra-high Sensitivity Imaging of Breast Cancer In-vivo

Adam de la Zerda, Sunil Bodapati, Shay Keren, Cristina Zavaleta, Robert Teed, Zhuang Liu, Scott Tabakman, Srikant Vaithilingam, Xiaoyuan Chen, Butrus T. Khuri-Yakub, Hongjie Dai, Sanjiv Sam Gambhir

Background and objectives: Photoacoustic imaging is an emerging technology that provides non-invasive imaging at high spatial resolution and depth of penetration. Here we demonstrate photoacoustic molecular imaging, by designing a family of photoacoustic agents that selectively bind to molecular targets in tumors in living mice. Furthermore, we show the ability to resolve the signals of two imaging agents, thereby allowing multiplexing studies.

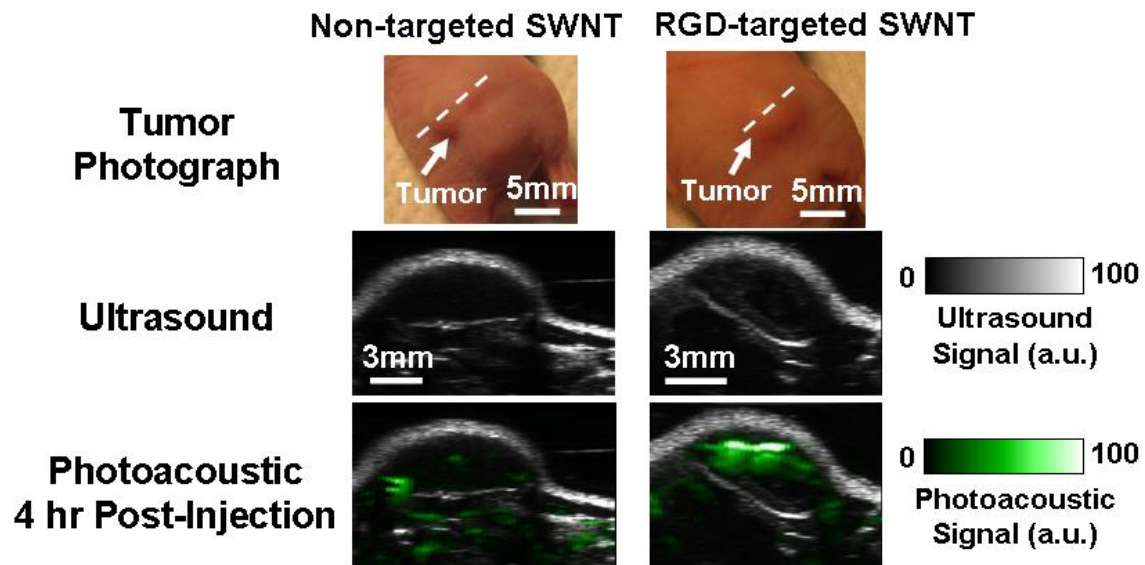
Methods: We synthesized imaging agents based on a single walled carbon nanotube (SWNT) conjugated with polyethylene-glycol-5000 connected to Arg-Gly-Asp (RGD) peptide to target the $\alpha_v\beta_3$ integrins in tumor vasculature. The SWNT surface was conjugated with optical dyes including QSY₂₁ and Indocyanine Green (ICG), rendering the SWNTs unique optical spectra. Finally, we built a high resolution near infra-red photoacoustic system for mice imaging.

Results: We measured the minimal detectable concentration of the dye-enhanced SWNTs in living mice to be 170 pM at a spatial resolution of 200 μ m and depths of 3-4 cm. This represents over two orders of magnitude improvement in both sensitivity and spatial resolution over conventional optical imaging techniques. The particles showed a strong photoacoustic signal that is linear to their concentration and independent of the RGD conjugation. Cell-uptake studies using U87 cells (that express $\alpha_v\beta_3$ on the cell membrane) showed 75% higher binding of RGD-targeted SWNT as compared with untargeted SWNTs.

We then showed that when RGD-targeted SWNTs are administered to tumor-bearing mice ($n = 4$) via the tail vein, they selectively bind to the $\alpha_v\beta_3$ integrins, producing a three-dimensional photoacoustic image of their distribution in the tumor (Fig. 1). Control untargeted particles showed 8-times lower photoacoustic signal in the tumor post-injection ($p < 0.001$). These results were verified ex-vivo using a Raman microscope that is sensitive to the SWNTs Raman signal. (de la Zerda et al, *Nature Nanotechnology*, 3, 557, 2008)

Finally, we showed that the dye-SWNT particles (QSY₂₁- and ICG-SWNTs) allow multiplexing studies and can be targeted to tumors in living mice (de la Zerda et al, *Nano Letters*, 10, 6, 2010; de la Zerda et al, *Nano Letters*, in review).

Conclusion: We presented the first demonstration of photoacoustic molecular imaging and synthesized a family of imaging agents that allow the imaging of multiple molecular activities in tumor-bearing mice. While current breast imaging is limited primarily to anatomical features, photoacoustic molecular imaging provides molecular information in high resolution that may allow an early assessment of tumor's response to neoadjuvant therapy.



RGD-targeted SWNTs administered intravenously to living mice produced significantly higher photoacoustic signal in tumor compared to mice injected with non-targeted SWNTs.